Supporting Information

Benzoselenadiazole Fluorescent Probes – Near IR Optical and Ratiometric Fluorescence Sensor for Fluoride Ion

Chinnusamy Saravanan[†], Shanmugam Easwaramoorthi, [‡] Hsiow Chuen-Yo,[†] Karen Wang[†], Michitoshi Hayashi[†]and Leeyih Wang[*, †]

[†]Centre for Condensed Matter Sciences, National Taiwan University, Taipei, 10617 Taiwan (R.O.C.);

[‡]Chemical Laboratory, CSIR-Central Leather Research Institute (CLRI), Adyar, Chennai 600 020, India

1. General information

All the starting materials, reagents (Aldrich) and solvents were AR grade purchased either from TEDIA or Mallinckrodt and used without any further purification. Reactions were monitored by thin layer chromatography using Merck TLC Silica gel 60 F254. Silica gel column chromatography was performed over Merck Silica gel 60 (particle size: 0.040-0.063 mm, 230-400 mesh ASTM). ^{1}H and ^{13}C NMR spectra were recorded on a BRUKER SPECTROSPIN-400 MHz spectrometer at room temperature using $CDCl_3$ or DMSO-d_6 as the solvent, and the solvent signal was adopted as an internal standard. The UV-Vis spectra were measured using a Jsaco-MD-2010 spectrophotometer. Fluorescence spectra were measured using Jobin Yvon- Fluorolog-TAU-3 and CARY-Eclipse spectrofluorimeter.

2. UV-Vis and Fluorescence titrations

Solutions of **TBS-HN** (3x 10^{-5} M) were prepared using commercially available DMSO. The tetrabutylammonium fluoride salt (0.06 M) was also dissolved in the same DMSO. 2 mL of **TBS-HN** was pipetted out into a cuvette and an initial UV-vis spectrum was recorded. Then, the corresponding F^- solution was added to the receptor solution in the cuvette from 4 equivalents of receptors concentrations to required concentration for saturation level. Now, the concentrations of receptors and anions in the cuvette were calculated from the total volume of the solution in the cuvette. Errors are within 10% in all cases. The same calculations were also used for the fluorescence titrations experiment. The UV-visible absorption and fluorescence spectra show linear behaviour with respect to the receptor concentration (SI, Figure S7)

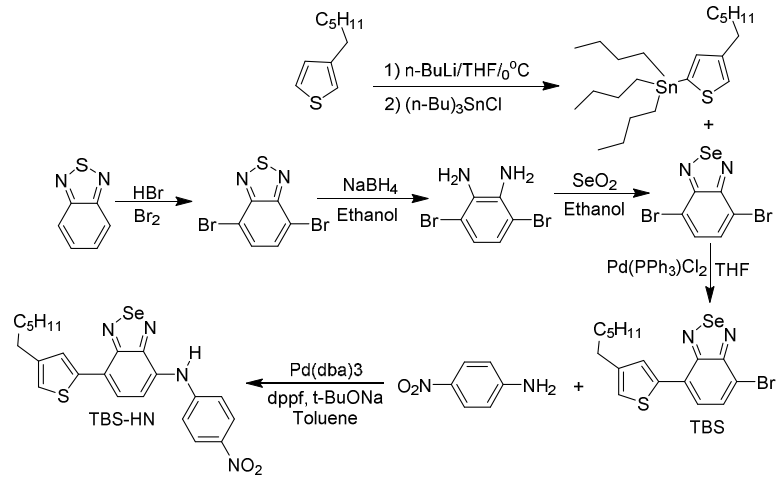

Scheme S1 Synthetic routes for **TBS-HN**

3. Synthesis

3.1 Synthesis of TBS

$PdCl_2(PPh_3)_2$ was added to a solution of 4,7-dibromo-2,1,3-benzoselenadiazole (1.29 g. 4.38 mmol) and tributyl-(4-hexyl-2-thienyl)stannane (2 g, 4.38 mmol) in THF. The mixture was refluxed under nitrogen for 24 h and then allowed to cool to room temperature. After the removal of the solvent under reduced pressure, the residue was purified by column chromatography on silica gel (40% CH_2Cl_2 in hexane) gave the compound (yield: 40%) as orange coloured solid. ^{1}H NMR (400 MHz, $CDCl_3$): δ_H 1.75-0.90 (m, 11H, aliphatic chain), 2.71 (t, 2H, Ar-$\underline{CH_2}$-CH_2-), 7.08 (s, 1H, Ar), 7.68 (d, 2H, Ar), 7.82 (d, 1H, Ar), 7.96 (s, 1H, Ar) ppm. ^{13}C NMR (400 MHz, $CDCl_3$): δ_C 14.11, 22.63,29.03, 30.46, 30.61, 31.69, 112.05, 122.06, 125.53, 127.35, 129.62, 132.23, 138.08, 144.51, 151.79, 153.79 ppm.

3.2 Synthesis of TBS-HN

Tris(dibenzylideneacetone)dipalladium(0) (11 mg), 1,1′-bis(diphenylphosphino) ferrocene (8.5 mg) and sodium tert-butoxide (225 mg) was added to the solution of

TBS (0.64 g. 1.7 mmol), 4-nitroaniline (0.25 g, 1.7 mmol) in 50 mL of toluene and refluxed (110-106 °C) for 24 h and cooled to room temperature. The solids were filtered off and washed with 250 mL of toluene. Then the filtrates were collected together, washed with water, brine solution and dried over anhydrous $MgSO_4$. The solvent was removed under reduced pressure and the crude product was purified by column chromatography (40 % CH_2Cl_2 in hexane) gave the red coloured solid with the yield of 63%. ^{1}H NMR (400 MHz, $CDCl_3$): δ_H 1.73-0.92 (m, 11H, aliphatic chain), 2.69 (t, 2H, Ar-CH_2-CH_2-), 7.00 (s, 1H, Ar), 7.26 (d, 2H, Ar), 7.36 (d, 1H, Ar), 7.73 (a, 2H, Ar), 7.80 (s, 1H, -N-H), 8.24 (d, 2H, Ar) ppm. ^{13}C NMR (400 MHz, $CDCl_3$): δ_C 14.13, 22.66, 29.07, 30.47, 30.70, 31.72, 110.31, 116.53, 120.32, 126.03, 126.56, 127.91, 131.23, 138.91, 141.42, 144.32, 146.98, 148.97, 152.53 ppm.

3.3 Synthesis of TBS-MN

The DMSO solution of tetrabutylammonium fluoride hydrate (377 mg, 1.44 mmol) was added to the solution of TBS-HN (100 mg, 0.21 mmol) in DMSO at room temperature over a period of 5 min and stirred further for 10 min followed by CH_3I (0.42 mmol) was added to the reaction mixture. After 10 minutes, the solution was poured into water and extracted by ethyl acetate, washed with water and brine solution. The solvent was removed and purified by column chromatography gave the yellow coloured solid with the yield of 96%. ^{1}H NMR (400 MHz, $CDCl_3$): δ_H 1.72-0.88 (m, 11H, aliphatic chain), 2.70 (t, 2H, Ar-CH_2-CH_2-), 3.57 (s, 3H, N-CH_3), 6.72 (d, 2H, Ar), 7.08 (s, 1H, Ar), 7.42 (d, 1H, Ar), 7.77 (d, 1H, Ar), 7.90 (s, 1H, Ar), 8.08 (d, 2H, Ar) ppm. ^{13}C NMR (400 MHz, $CDCl_3$): δ_C 14.11, 22.63, 29.03, 29.70, 30.47, 30.63, 31.70, 40.38, 113.02, 122.32, 125.38, 125.76, 127.44, 128.58, 129.47, 137.66, 138.70, 138.94, 144.22, 153.72, 157.15, 158.99 ppm.

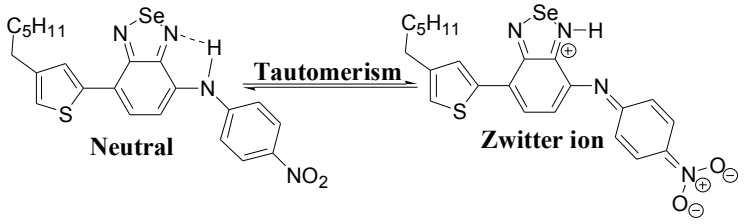

Scheme S2. Plausible mechanism for the ESIPT process

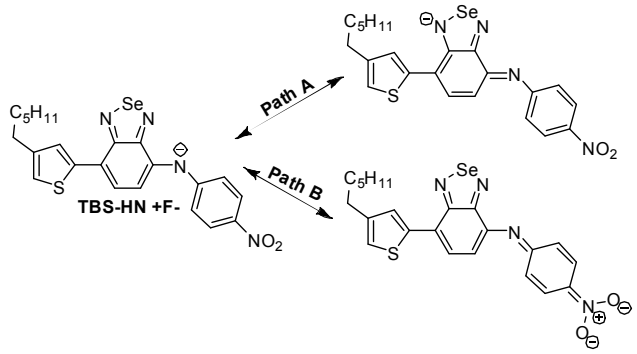

Scheme S3. Plausible route for the migration of electron after deprotonation of amine proton by F- in DMSO.

Table S1. Calculated[1] surfaces of HOMO-1, HOMO, LUMO, and LUMO+1 (the isovalue was set to 0.02 and the coarse cube grid was used. The electronic structure is different between neutral form and charge form: in particular, the origin of the HOMOs of these two forms is quite different).

	HOMO-1	HOMO	LUMO	LUMO+1
TBS-HN (Neutral form)	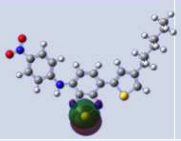	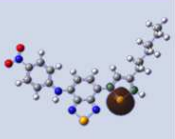	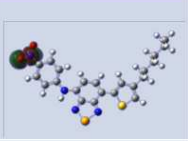	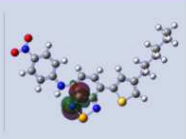
TBS-HN +F- (Charged form)	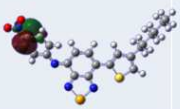	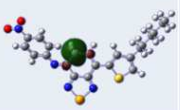	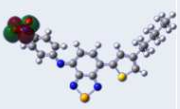	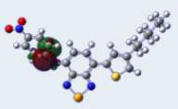

Table S2. The origin of the first three electronic transitions of the two forms (major contribution of each electronic transition is shown with its ratio (%) and orbital origin).

Electronic transition	TBS-HN (Neutral form)	TBS-HN+F⁻ (Charged form)
1st	96.8% HOMO → LUMO 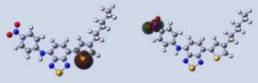	97.5 % HOMO → LUMO 
2nd	95.6% HOMO → LUMO+1 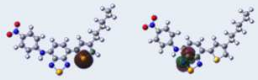	84.1 % HOMO → LUMO+1 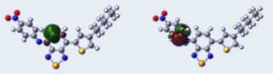
3rd	95.3 % HOMO-1 → LUMO 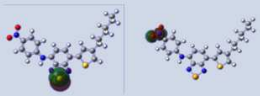	80.8% HOMO-1 → LUMO 

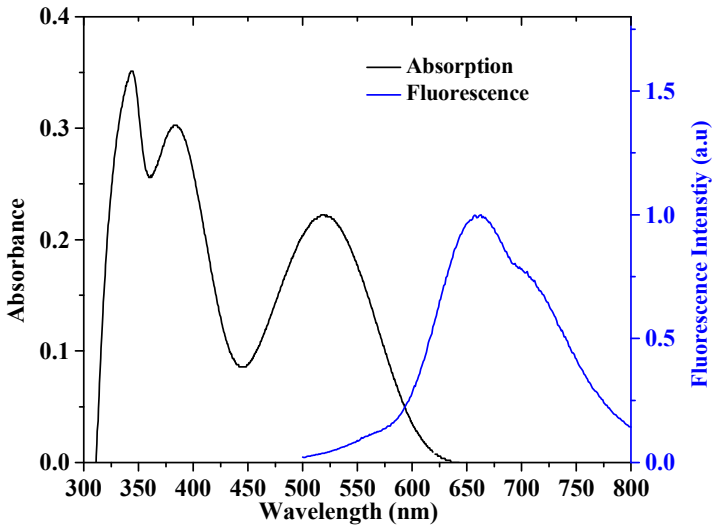

Figure S1. Absorption, fluorescence spectra of **TBS-HN** in toluene (Abs. – 344, 383, 520 nm; Flu. – 662, 705 (s) nm; Stoke's shift 4125 cm^{-1} (140 nm).

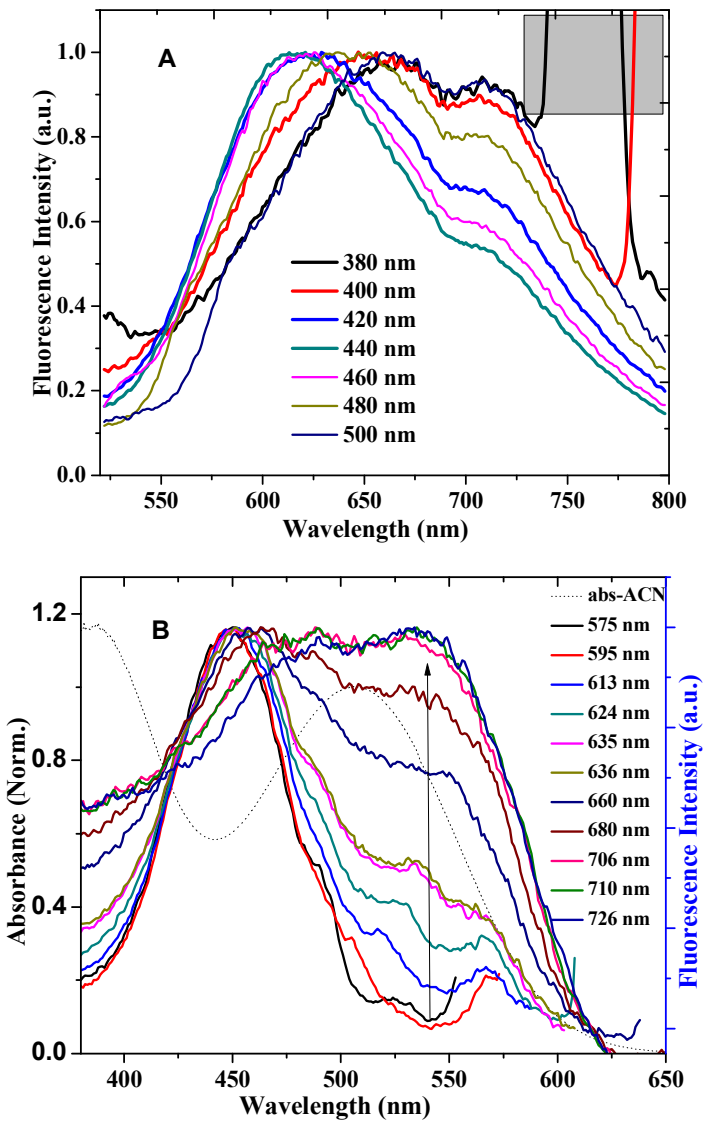

Figure S2. A) Fluorescence spectra of **TBS-HN** in ACN upon excited with various wavelengths. (The peak marked in grey rectangle is due to second order scattering) B) Excitation spectra of **TBS-HN** in ACN with various excitation wavelengths. Dotted line – Uv-visible absorption Spectrum

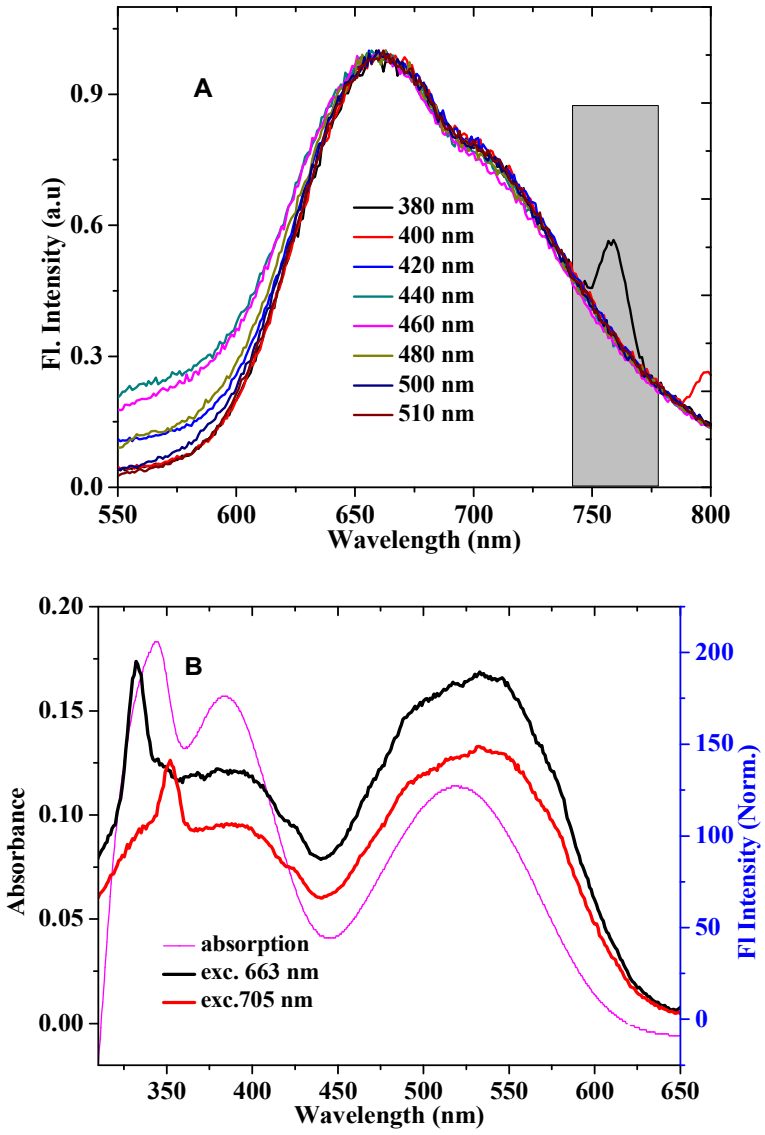

Figure S3. A) Fluorescence spectra of **TBS-HN** in toluene upon excitation with various wavelengths (The peak marked in grey rectangle is due to second order scattering). B) Absorption and excitation spectra of **TBS-HN** in toluene

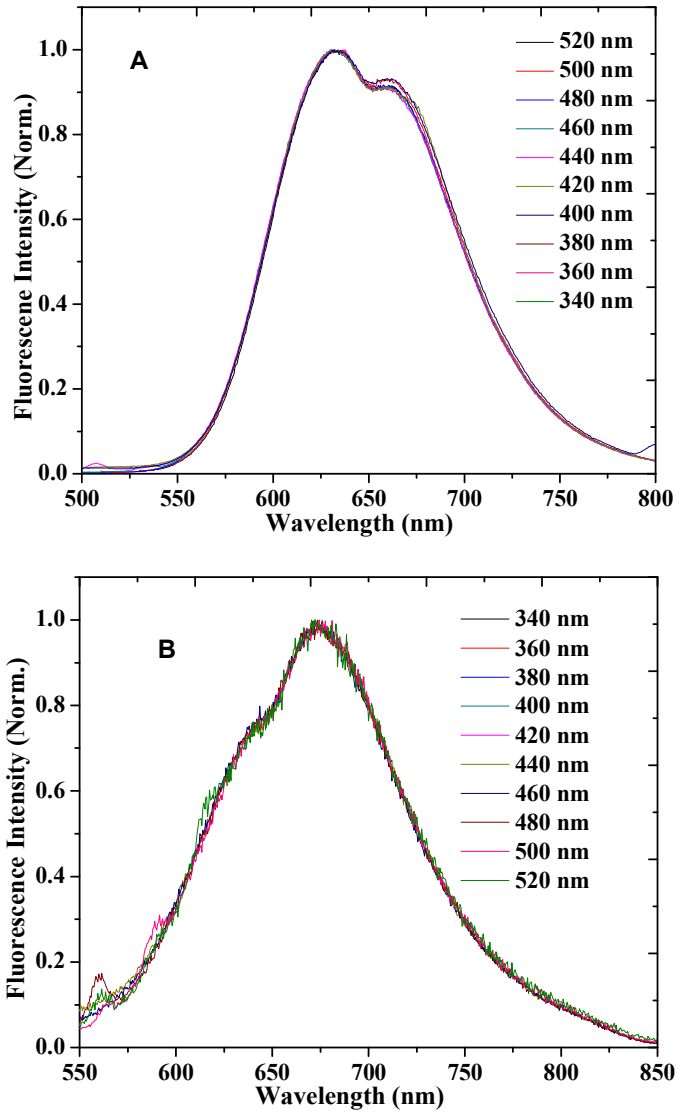

Figure S4. Fluorescence spectra of **TBS-MN** in A) toluene and B) acetonitrile measured at various excitation wavelengths

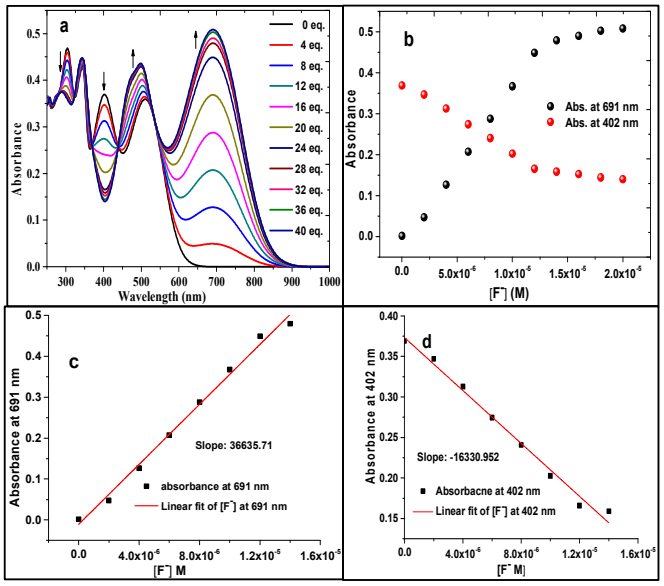

Figure S5. a) UV-vis absorption spectra of **TBS-HN** ($3x10^{-5}$ M) upon addition of various equivalents of F^- in DMSO, b) Plot of absorbance change at 691nm and 402 nm versus fluoride ion concentration. Plot of absorbance at c) 691 nm & d) 402 nm versus fluoride ion concentration at lower fluoride concentration levels.

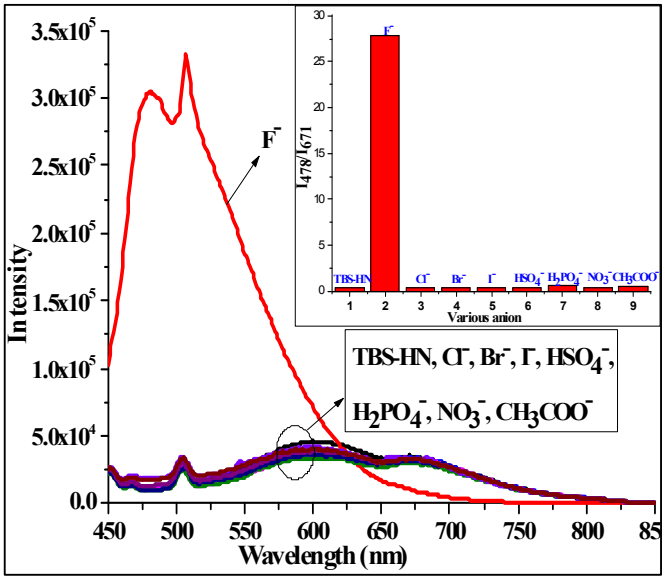

Figure S6. Fluorescence spectra of **TBS-HN** ($3x10^{-5}$ M) upon addition of 150 equivalents of various anions in the form their TBA salts in DMSO.

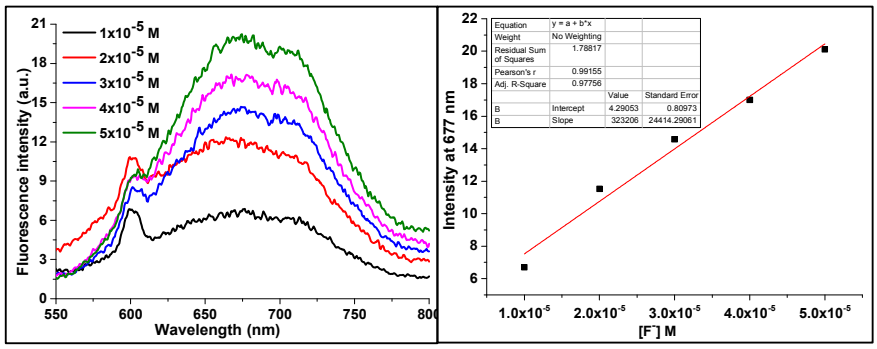

Figure S7. Fluorescence spectra of TBS-HN in DMSO at various concentrations.

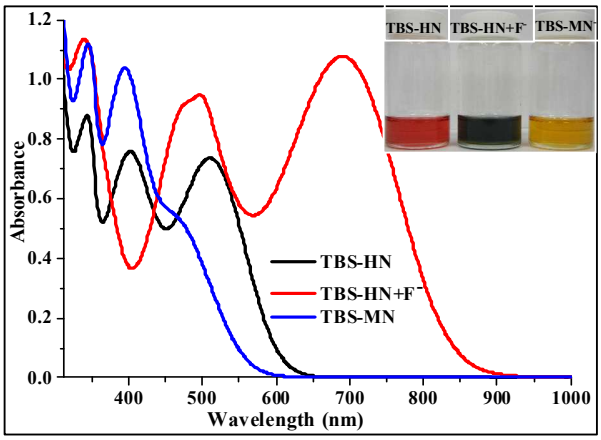

Figure S8. UV-vis absorption spectra TBS-HN ($3x10^{-5}$ M) TBS-HN+100 equivalents of F^- and TBS-HN+100 equivalents of F^- + 4 equiv. of CH_3I (TBS-MN) in DMSO.

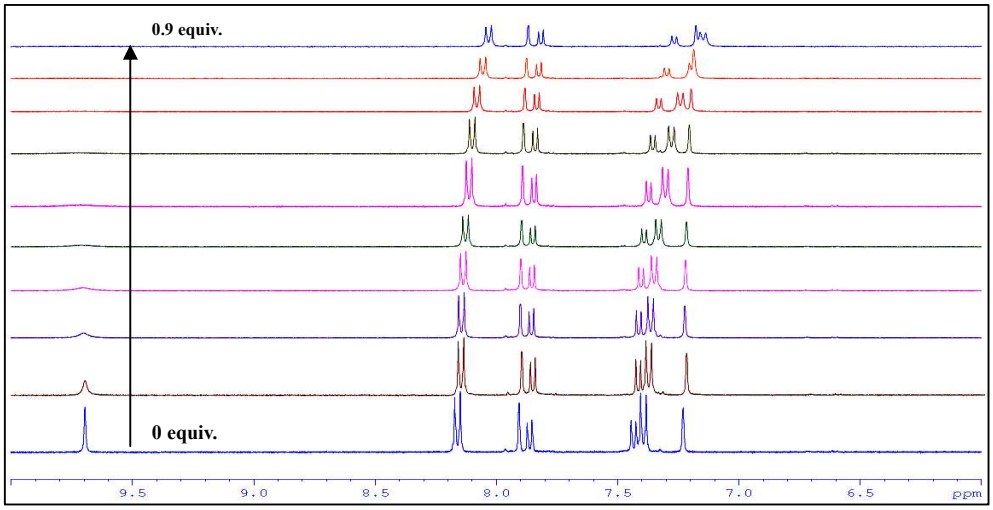

Figure S9. Partial ^{1}H NMR spectra (10-6 ppm region) of TBS-HN in the presence of various equivalents of F^{-} in DMSO-d_6.

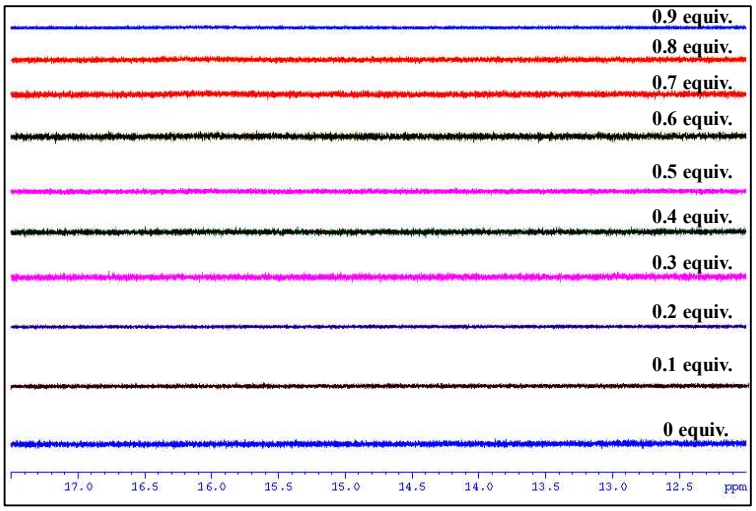

Figure S10. Partial ^{1}H NMR spectra (17.5-12 ppm) of **TBS-HN** in the presence of various equivalents of F^{-} in DMSO-d_6.

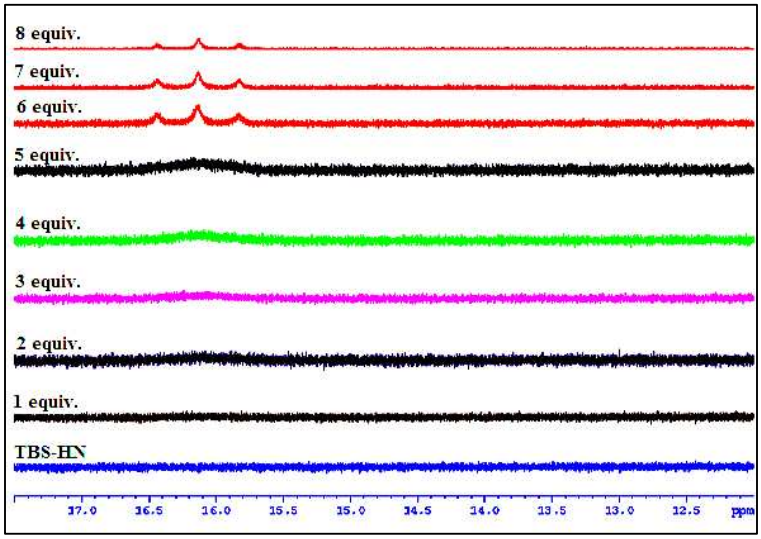

Figure S11. Partial ^{1}H NMR spectra (17.5-12 ppm region) of **TBS-HN** in the presence of various equivalents of F^{-} in DMSO-d_6.

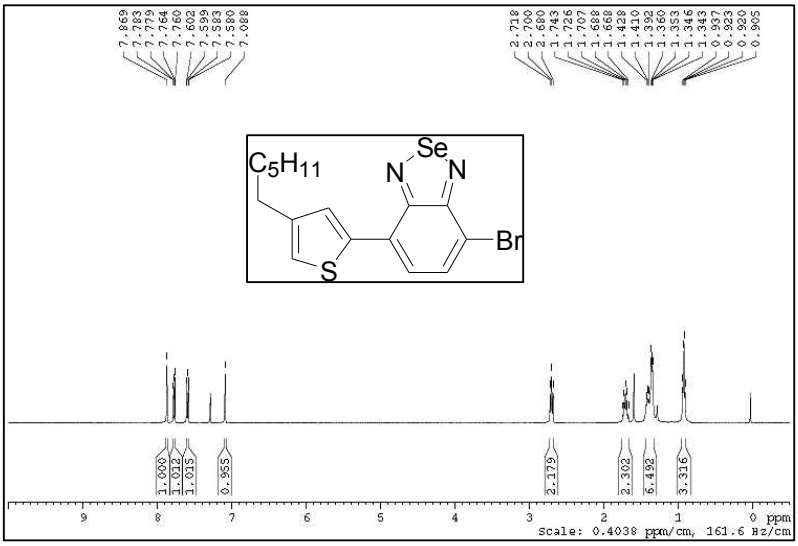

Figure S12 ^{1}H NMR spectrum of **TBS** in $CDCl_3$.

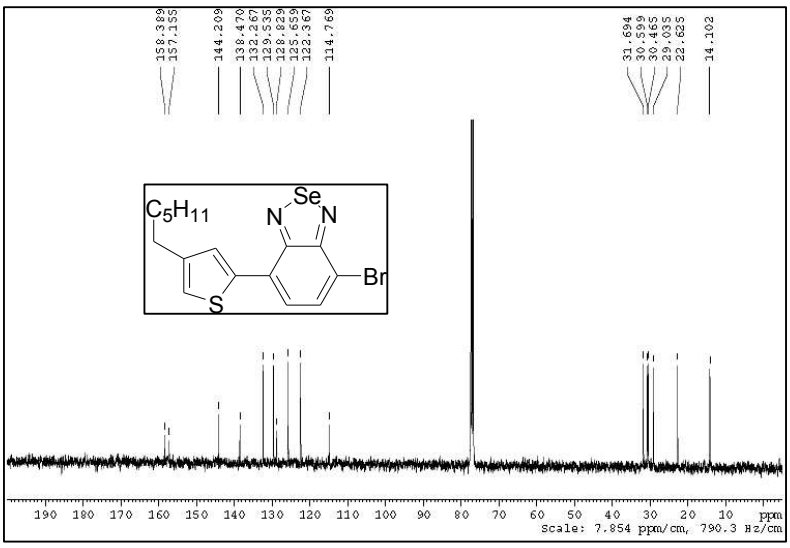

Figure S13 ^{13}C NMR spectrum of **TBS** in $CDCl_3$.

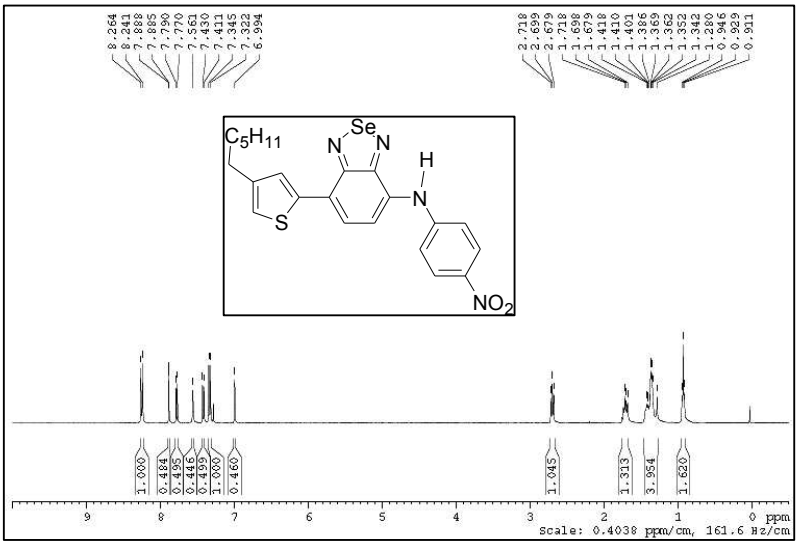

Figure S14 ^{1}H NMR spectrum of **TBS-HN** in $CDCl_3$.

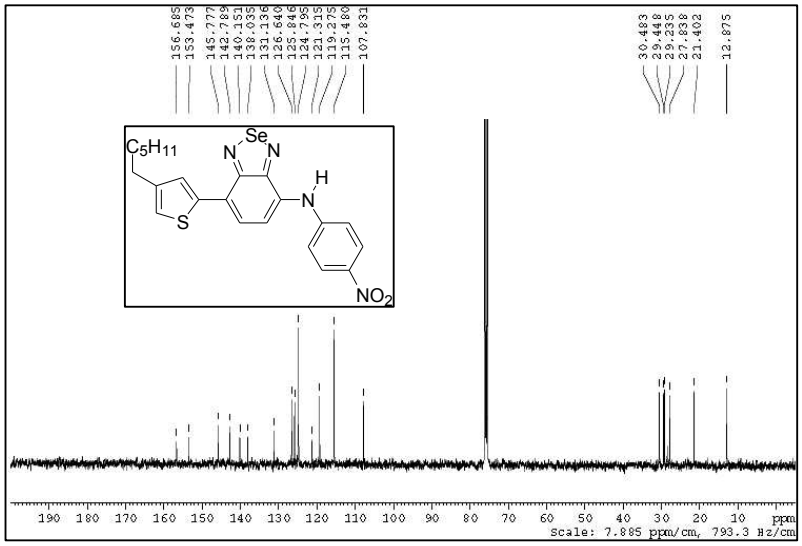

Figure S15 ^{13}C NMR spectrum of **TBS-HN** in $CDCl_3$.

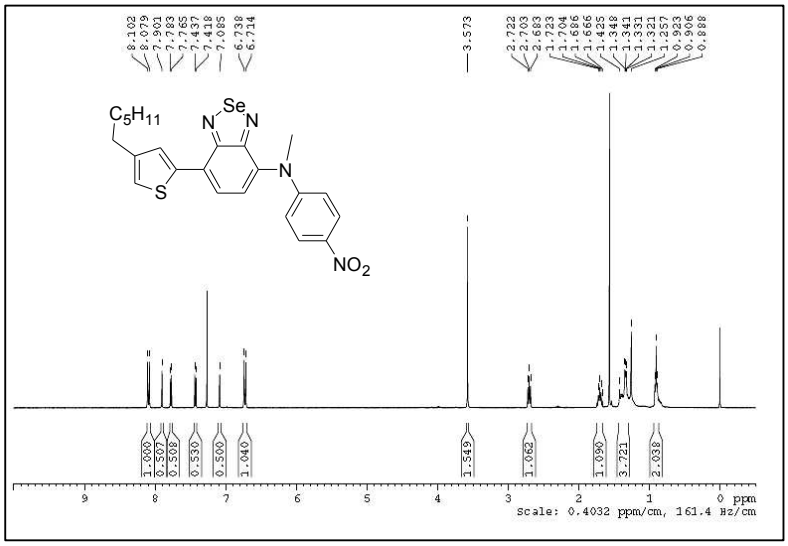

Figure S16 ^{1}H NMR spectrum of **TBS-MN** in $CDCl_3$

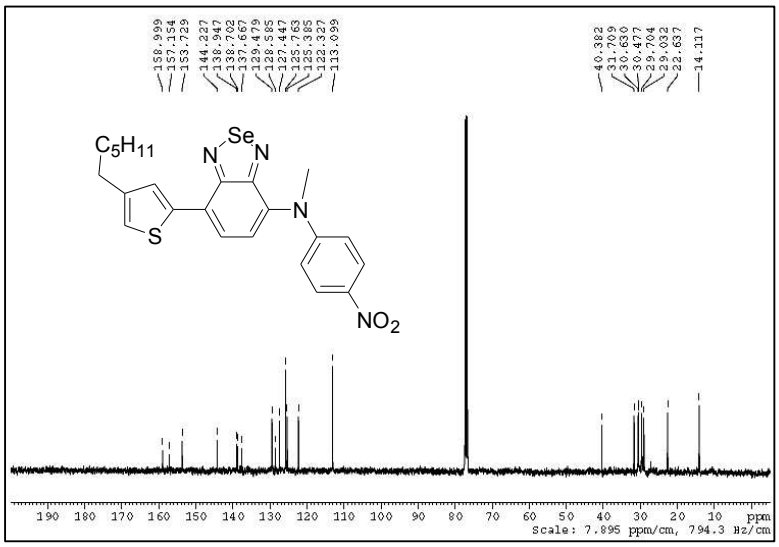

Figure S17 ^{13}C NMR spectrum of **TBS-MN** in $CDCl_3$

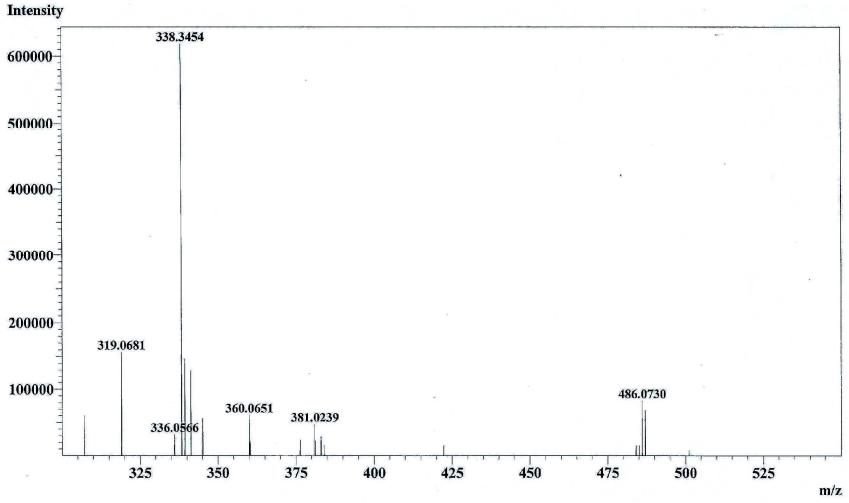

Figure S18 ESI-MS spectrum of **TBS-HN**. (Observed m/z = 486.07 and calculated m/z = 486.06 for $C_{22}H_{22}N_4O_2SSe$

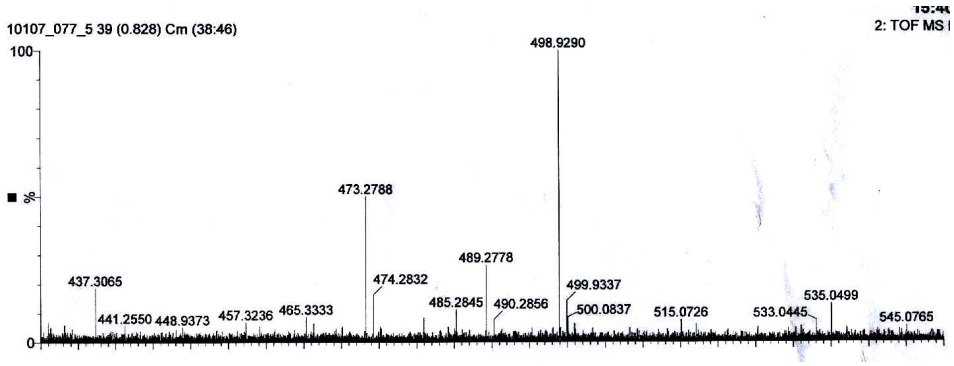

Figure S19 HRMS spectrum of **TBS-MN**. (Observed m/z = 498.9290 and calculated m/z = 499.4873 for $C_{23}H_{24}N_4O_2SSe$.

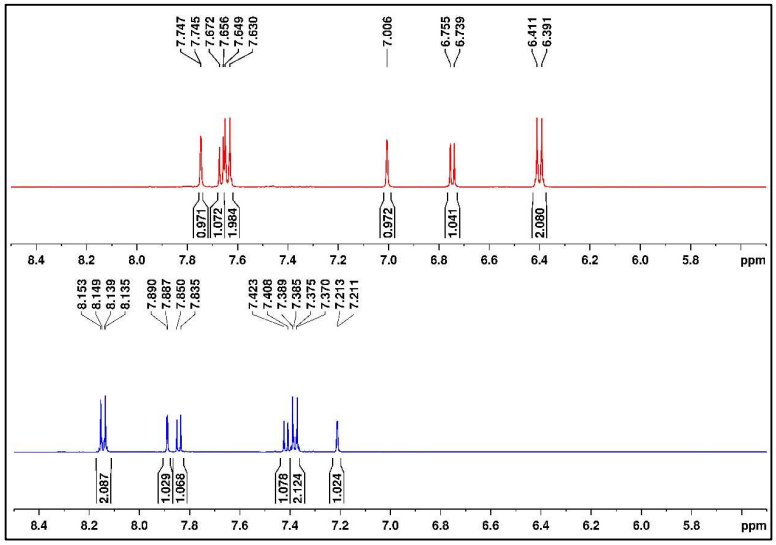

Figure S20 Partial ^{1}H NMR spectra of **TBS-HN** (bottom) and in the presence of 15 equivalents of F^- (top) in DMSO-d_6.

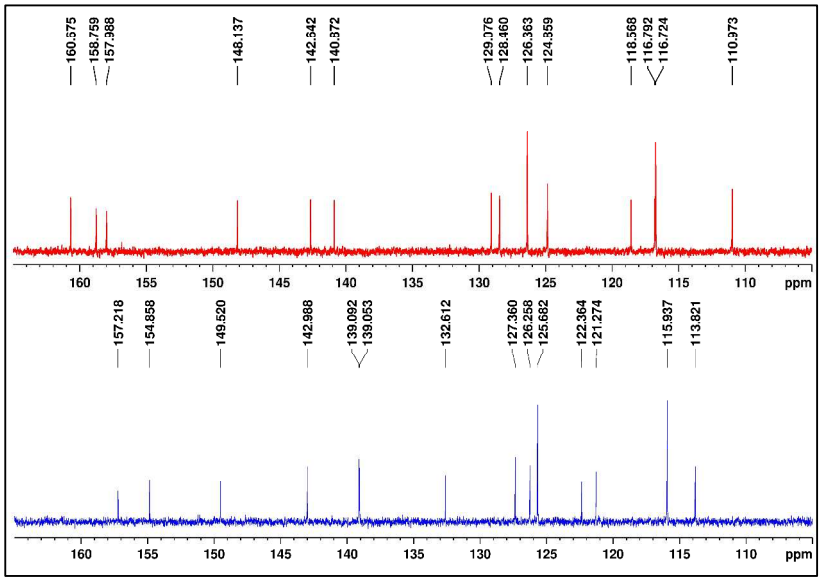

Figure S21 Partial ^{13}C NMR spectra of **TBS-HN** (bottom) and in the presence of 15 equivalents of F^- (top) in DMSO-d_6.

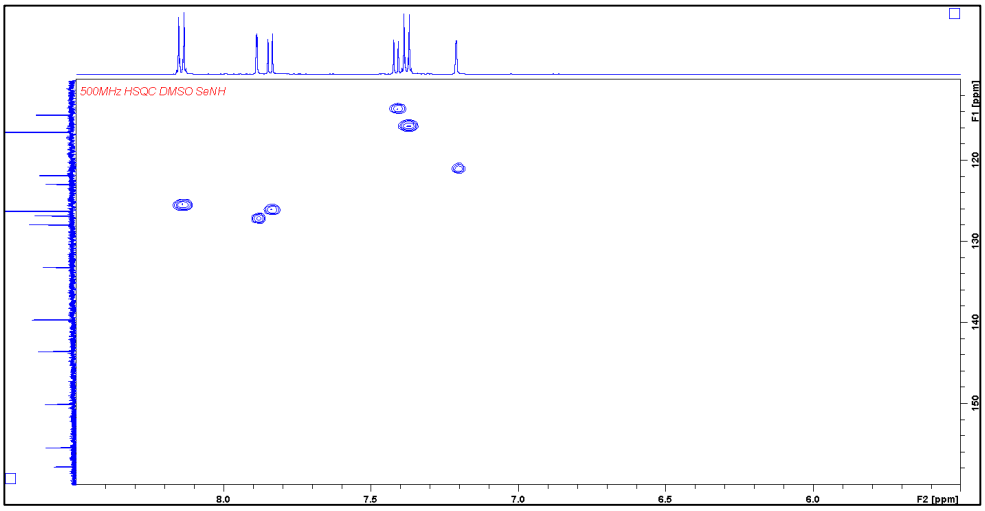

Figure 22 Partial 2D NMR (HSQC) spectrum of **TBS-HN** (DMSO-d_6, 600 MHz).

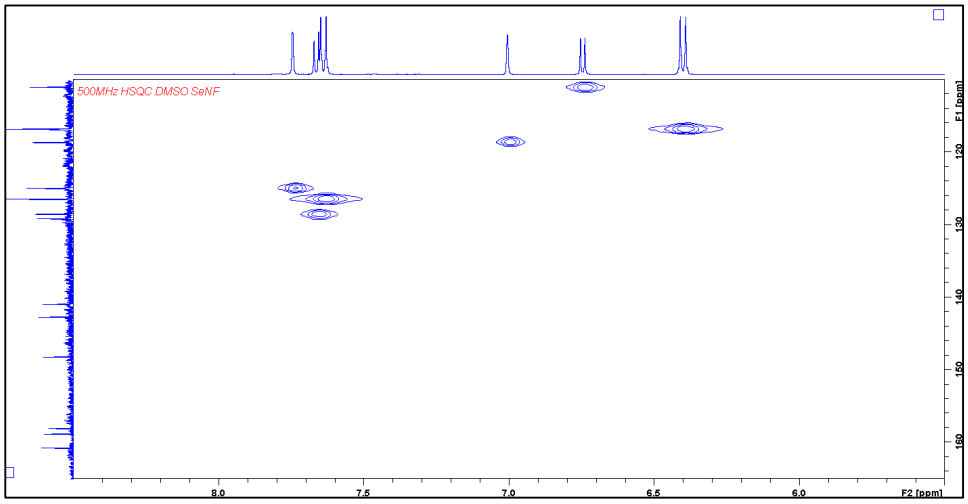

Figure 23 Partial 2D NMR (HSQC) spectrum of **TBS-HN** in the presence of 15 equivalents of F^- (DMSO-d_6, 600 MHz).

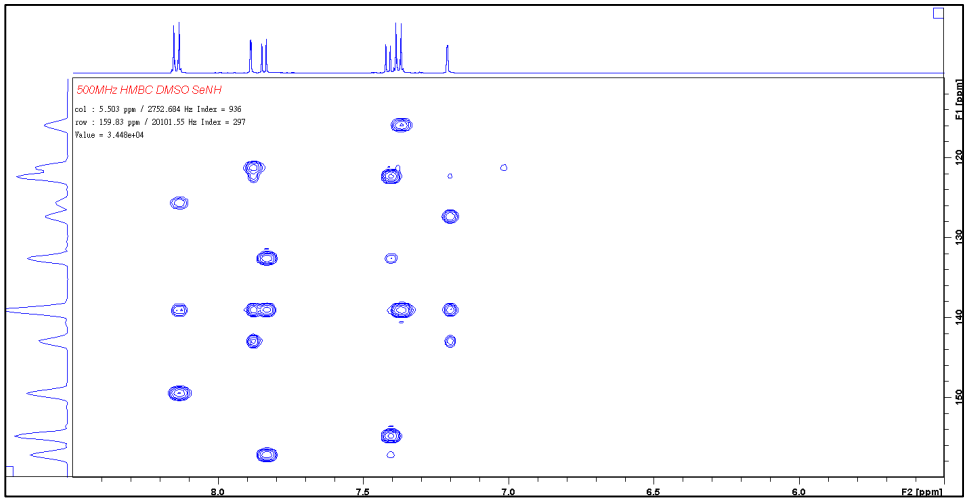

Figure 24 Partial 2D NMR (HMBC) spectrum of **TBS-HN** (DMSO-d_6, 600 MHz).

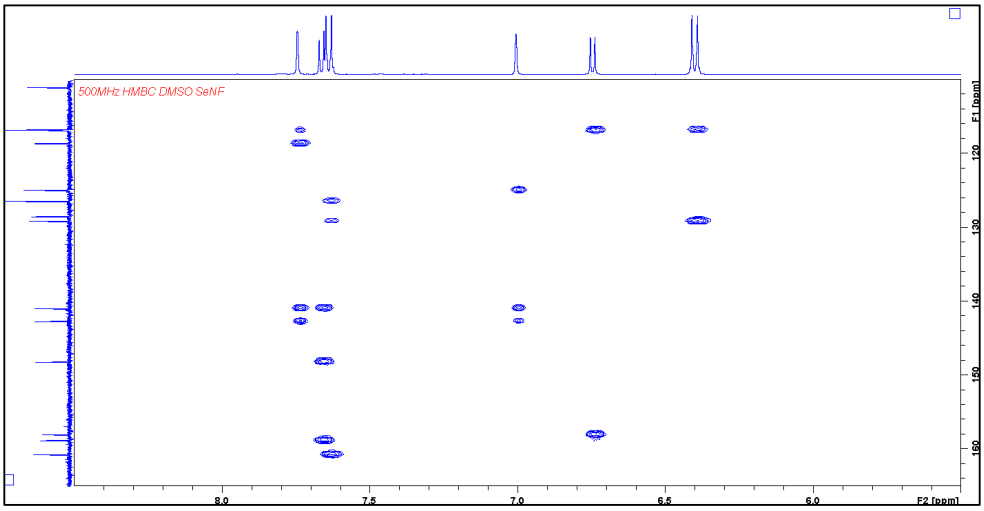

Figure 25 Partial 2D NMR (HMBC) spectrum of **TBS-HN** in the presence of 15 equivalents of F^- (DMSO-d_6, 600 MHz).

Reference

1. Gaussian 09, Revision B.1, Frisch, M. J.; Trucks, G. W.; Schlegel, H. B.; Scuseria, G. E.; Robb, M. A.; Cheeseman, J. R.; Scalmani, G.; Barone, V.; Mennucci, B.; Petersson, G. A.; Nakatsuji, H.; Caricato, M.; Li, X.; Hratchian, H. P.; Izmaylov, A. F.; Bloino, J.; Zheng, G.; Sonnenberg, J. L.; Hada, M.; Ehara, M.; Toyota, K.; Fukuda, R.; Hasegawa, J.; Ishida, M.; Nakajima, T.; Honda, Y.; Kitao, O.; Nakai, H.; Vreven, T.; Montgomery, Jr., J. A.; Peralta, J. E.; Ogliaro, F.; Bearpark, M.; Heyd, J. J.; Brothers, E.; Kudin, K. N.; Staroverov, V. N.; Kobayashi, R.; Normand, J.; Raghavachari, K.; Rendell, A.; Burant, J. C.; Iyengar, S. S.; Tomasi, J.; Cossi, M.; Rega, N.; Millam, J. M.; Klene, M.; Knox, J. E.; Cross, J. B.; Bakken, V.; Adamo, C.; Jaramillo, J.; Gomperts, R.; Stratmann, R. E.; Yazyev, O.; Austin, A. J.; Cammi, R.; Pomelli, C.; Ochterski, J. W.; Martin, R. L.; Morokuma, K.; Zakrzewski, V. G.; Voth, G. A.; Salvador, P.; Dannenberg, J. J.; Dapprich, S.; Daniels, A. D.; Farkas, Ö.; Foresman, J. B.; Ortiz, J. V.; Cioslowski, J.; Fox, D. J. Gaussian, Inc., Wallingford CT, 2009.